energies

MDPI

Article

Array of Active Shielding Coils for Magnetic Field Mitigation in Automotive Wireless Power Transfer Systems

Silvano Cruciani [1], Tommaso Campi [2,*], Francesca Maradei [2] and Mauro Feliziani [3]

[1] Department of Industrial Engineering, Tor Vergata University of Rome, 00133 Rome, Italy; silvano.cruciani@uniroma2.it
[2] Department of Astronautic, Electrical and Energy Engineering, Sapienza University of Rome, 00184 Rome, Italy; francesca.maradei@uniroma1.it
[3] Department of Industrial and Information Engineering, University of L'Aquila, 67100 L'Aquila, Italy; mauro.feliziani@univaq.it
* Correspondence: tommaso.campi@uniroma1.it

Abstract: This paper deals with the mitigation of magnetic field levels produced by a wireless power transfer (WPT) system to recharge the battery of an electric vehicle (EV). In this work, an array of active coils surrounding the WPT coils is proposed as a mitigation technique. The theory and new methodological aspects are the focus of the paper. Magnetic field levels in the environment are calculated numerically without and with the presence of an array of active coils in a stationary WPT system for automotive applications. By the proposed mitigation method, the field levels beside the vehicle are significantly reduced and comply with the reference levels (RLs) of the ICNIRP 2010 guidelines for human exposure to electromagnetic fields and the magnetic flux density limits proposed by ISO 14117 for electromagnetic interference (EMI) in cardiac implantable electronic devices (CIEDs).

Keywords: active coil; cardiac implantable electronic device (CIED); electromagnetic compatibility (EMC); electromagnetic field (EMF) safety; electromagnetic interference (EMI); magnetic field; near field; shielding; wireless power transfer (WPT)

Citation: Cruciani, S.; Campi, T.; Maradei, F.; Feliziani, M. Array of Active Shielding Coils for Magnetic Field Mitigation in Automotive Wireless Power Transfer Systems. *Energies* **2024**, *17*, 4233. https://doi.org/10.3390/en17174233

Academic Editor: Haifeng Dai

Received: 13 June 2024
Revised: 10 July 2024
Accepted: 21 August 2024
Published: 24 August 2024

1. Introduction

Electric vehicles (EVs) bring significant advances in transportation technology, promising a green and more sustainable future. For the widespread adoption of electrified transportation on wheels, an efficient and convenient charging infrastructure is necessary. Wireless power transfer (WPT) based on resonant inductive coupling is the most promising technology for its potential and for the elimination of the plug-in physical connections [1–8]. However, the implementation of this technology raises concerns about the strong magnetic fields emitted into the environment from WPT systems, which could pose potential health risks to occupants and nearby people and interfere with sensitive electronic equipment and infrastructures [9–11]. Therefore, WPT systems are critical for the electromagnetic field (EMF) safety of exposed individuals and the electromagnetic compatibility/electromagnetic interference (EMC/EMI) to electric/electronic devices. Such issues can be particularly critical in densely populated urban environments where many electric vehicles may be located. Consequently, there is an urgent need to develop effective mitigation techniques to minimize the magnetic field emitted from automotive WPT systems.

A potential solution for magnetic field mitigation consists in using additional active or passive shielding coils (or loops) that generate a magnetic field opposite to that created by the WPT system. In a passive configuration, the shielding loop is terminated on an impedance, and the current flowing through it is induced by the incident magnetic field produced by the WPT coils according to Faraday's law [11–18]. When the passive loop is properly terminated, typically on a capacitance, the magnetic field produced by the

shielding coil can oppose the incident field. However, achieving the desired current (both in magnitude and phase) in the passive shielding coil is not always possible, which can result in suboptimal field mitigations.

Active shielding coils provide a practical and cost-effective solution to the challenges posed by magnetic field emissions from WPT systems [19–28]. Unlike passive ones, active shielding coils have an independent power supply that allows the regulation of the magnitude and phase of the current through appropriate control mechanisms. While the theory behind active shielding coils is well established, this work introduces an innovative approach, using an array of active shielding coils to mitigate the magnetic field in a wireless charging system for EVs. The design of active shielding coils is particularly challenging since a successful field mitigation often negatively impacts the power transfer efficiency. Strategically feeding an array of active shielding coils around the EV WPT charging system helps reduce magnetic field levels while maintaining a high power transfer efficiency and electrical performance [4,13]. The main novelty of the proposed work compared with past works on active shielding lies in the possibility of selecting the optimal power supply for a shielding system composed of N independent coils. This allows for great flexibility and adaptability to any type of WPT system.

The paper is focused on the methodological aspects of an array of active shielding coils and is organized as follows. First, a comprehensive analysis of using an array of active shielding coils for automotive wireless power systems is presented. We begin by providing an overview of the WPT theory and the sources of magnetic field emissions in WPT systems. Next, we discuss the design considerations and optimization techniques for integrating active shielding coils into the WPT infrastructure. Furthermore, we present simulation results to demonstrate the effectiveness of the proposed approach in reducing magnetic field emissions while ensuring high power transfer efficiency. Through a comparative analysis of different array configurations, we highlight the advantages and limitations of the different solutions developed for a WPT system similar to that standardized by SAE J2954 [29].

Additionally, we address practical implementation challenges and considerations, including cost-effectiveness, scalability, and compatibility with existing WPT standards and infrastructure. By providing insights into the performance and feasibility of using an array of active cancellation loops, this paper aims to contribute to the development of robust and environmentally friendly charging solutions for the electric mobility infrastructure.

2. Materials and Methods

A two-coil WPT system with circular coils, as specified by the SAE J2954 standard, is considered and assumed to be the source of the magnetic field [13]. The array of active shielding coils is designed to be placed around and coplanar with the primary WPT coil. This configuration is chosen because the primary coil is considered the main source of magnetic field emissions in the environment, and installing active shielding coils on the ground is straightforward.

One possible configuration of the shielding coils is shown in Figure 1. In this configuration, the shielding structure consists of an array of $N-2$ active shielding coils. The equivalent circuit can be modeled by N-coupled circuits:

- One primary coil, known in the SAE standard as the ground assembly (GA) coil, represented by the self-inductance L_1 and self-resistance R_1;
- One secondary coil, known as the vehicle assembly (VA) coil, represented by the self-inductance L_2 and self-resistance R_2;
- $N-2$ active shielding coils. All N coils can be modeled with a self-inductance L_i and self-resistance R_i and are inductively coupled.

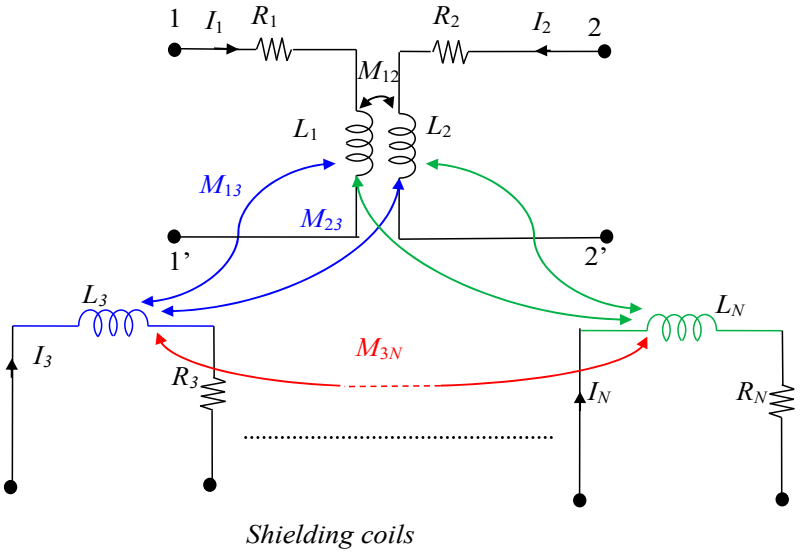

Figure 1. Equivalent circuit of a WPT system in the presence of $N-2$ shielding coils.

The circuit parameters of all N coils can be extracted using an electromagnetic field solver based on the finite element method (FEM). This field solver can also evaluate the magnetic field produced by the coil currents [4]. The numerical approach is employed due to the configuration complexity of the GA and VA coils, which include conductive and magnetic layers, as described in SAE J2954 [29].

The self- and mutual inductances of the N coils can be extracted from the magnetic energy, which is generally numerically calculated in the region under examination [4]. The self-inductance of the i-th coil is calculated as

$$L_i = \frac{2W_i}{I_i^2} \tag{1}$$

where W_i is the magnetic energy produced by the current I_i flowing in the i-th coil, while any other current in the other coils is zero (that is, $I_k = 0$, with $k \neq i$).

The mutual inductance M_{ik} between i-th and k-th coils is calculated by a two-step procedure using the following formula [4]:

$$M_{ik} = \frac{W_{ik}' - W_{ik}''}{2I_i I_k} \tag{2}$$

where

- W_{ik}' is the magnetic field energy obtained, assuming I_i and I_k are flowing in the i-th and k-th coils, respectively, while in the remaining coils, $I_h = 0$, with $h \neq i$ and $h \neq k$;
- W_{ik}'' is the magnetic field energy obtained, assuming the same current, I_i, is flowing in the i-th coil but an opposite current, $-I_k$, is flowing in the k-th coil, with no current applied to the other coils, $I_h = 0$, with $h \neq i$ and $h \neq k$.

The coil resistance, R_i, of the copper litz wire used for the i-th coil is obtained from the datasheet [30]. The extraction of this parameter through simulation for the litz wire is computationally impracticable or very intensive.

The N-coupled coils are described by an $N \times N$ impedance matrix $[Z]$, whose generic coefficient Z_{ik} is given by

$$Z_{ik} = \begin{cases} R_i + j\omega L_i \ \forall i = k \\ j\omega M_{ik} \ \ \forall i \neq k \end{cases} \tag{3}$$

Double-sided LCC compensation topology is adopted to operate the WPT system under resonant conditions according to the circuit shown in Figure 2, where an equivalent voltage source, V_0, in series with a source resistance, R_S, models the power electronic

converters upstream of the transmitting coil, and a load resistor, R_L, models the power electronic converters downstream of the receiving coil [4].

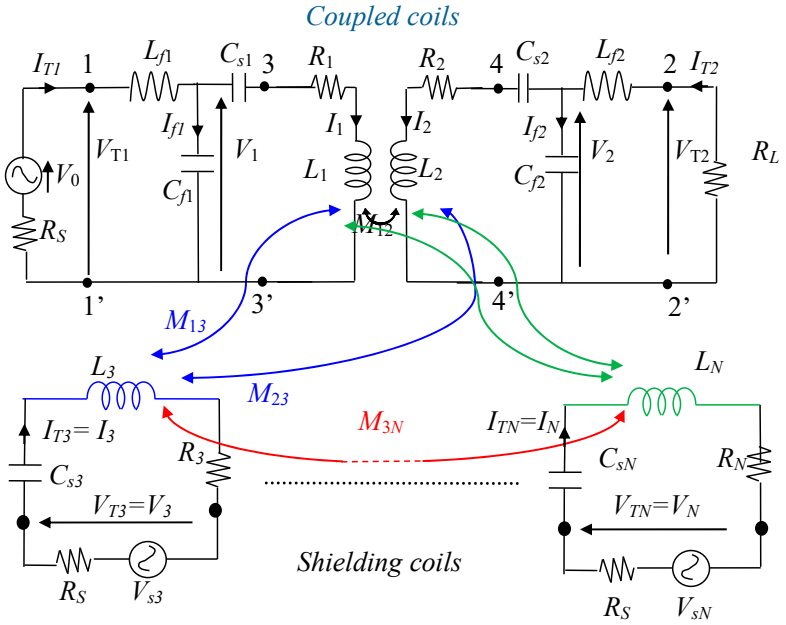

Figure 2. Equivalent simplified circuit of a WPT system LCC compensation and $N-2$ active shielding coils.

The values of the i-th shunt capacitance C_{fi} and series capacitance C_{Si} of the LCC networks are, respectively, given by

$$C_{fi} = 1/\left(\omega_0^2 L_{fi}\right)\ i \in \{1,2\} \tag{4}$$

$$C_{Si} = 1/\left(\omega_0^2\ \left(L_i - L_{fi}\right)\right)\ i \in \{1,2\} \tag{5}$$

where L_{fi} is the series inductance of the LCC compensation network and ω_0 is the resonant angular frequency.

To improve the efficiency of shielding coils, compensation capacitors $C_{Si} = 1/\left({\omega_0}^2 L_i\right)$ with $i = 3, N$ are connected in series, and a simplified excitation circuit is adopted for each shielding coil based on the series of a voltage source, V_{sk}, with a source resistance, R_S, assuming that all the sources have the same resistance as the transmitting coil.

For the terminations, the following relation holds:

$$[V_S] = [V_T] + [Z_T][I_T] \tag{6}$$

where $[V_S] = [V_0\ 0\ V_{s3} \ldots V_{sN}]^t$ is the vector of the voltage sources, $[V_T] = [V_{T1}\ V_{T2} \ldots V_{TN}]^t$ is the vector of the terminal voltages, $[I_T]$ is the vector of the N-port terminal currents, and $[Z_T]$ is the $N \times N$ matrix of the terminal impedances given by

$$[Z_T] = \begin{bmatrix} R_S & 0 & \cdots & 0 \\ 0 & R_L & \cdots & 0 \\ \vdots & \vdots & \ddots & \vdots \\ 0 & 0 & \cdots & R_S \end{bmatrix}. \tag{7}$$

Adopting the notation shown in Figure 2, the terminal voltages can also be expressed as

$$\begin{cases} V_{T1} = V_1 + j\omega L_{f1} I_{T1} \\ V_{T2} = V_2 + j\omega L_{f2} I_{T2} \\ V_{T3} = V_3 \\ \vdots \\ V_{TN} = V_N \end{cases} \quad (8)$$

or in compact matrix form as

$$[V_T] = [V] + [Z_f][I_T] \quad (9)$$

where the impedance matrix $[Z_f]$ is diagonal, with non-zero terms only for i = 1, 2 (i.e., WPT coils) given by

$$Z_{fii} = j\omega L_{fi}\ i \in \{1,2\}. \quad (10)$$

The voltage vector $[V]$ in (7) can be expressed as

$$[V] = \{[Z_C] + [Z]\}[I] \quad (11)$$

where the coefficients of matrix $[Z]$ are given by (1), and the matrix $[Z_C]$ is diagonal, with its coefficients given by

$$Z_{Cik} = \begin{cases} -j\frac{1}{\omega C_{Si}} \ \forall i = k \\ 0 \ \forall i \neq k \end{cases}. \quad (12)$$

Introducing (11) and (9) into (6) yields

$$[V_S] = \{[Z_C] + [Z]\}[I] + \left\{[Z_f] + [Z_T]\right\}[I_T]. \quad (13)$$

According to the Kirchhoff current law applied to the circuit in Figure 2, the following relation between the currents through the terminations and those through the coils can be derived as

$$\begin{cases} I_{T1} = I_1 + j\omega C_{f1} V_1 \\ I_{T2} = I_2 + j\omega C_{f2} V_2 \\ I_{T3} = I_3 \\ \vdots \\ I_{TN} = I_N \end{cases}, \quad (14)$$

which can also be written in compact matrix form as

$$[I_T] = [I] + [Y_f][V] \quad (15)$$

where the shunt admittance matrix $[Y_f]$ is diagonal, with non-zero terms only for i = 1,2 (i.e., WPT coils) given by

$$Y_{fii} = j\omega C_{fi}\ i \in \{1,2\}. \quad (16)$$

Introducing (11) in (15) yields

$$[I_T] = \left\{[1_N] + [Y_f]\{[Z_C] + [Z]\}\right\}[I] \quad (17)$$

where $[1_N]$ is the unit matrix of size N.

By introducing (17) into (13), the following relations between the voltage source vector and the coil current vector holds:

$$[V_S] = [Z_{eq}][I] \quad (18)$$

where the transfer impedance matrix $[Z_{eq}]$ is given by

$$[Z_{eq}] = [Y_{eq}]^{-1} = \left\{[Z_C] + [Z] + \left\{[Z_f] + [Z_T]\right\}\left\{[1_N] + [Y_f]\{[Z_C] + [Z]\}\right\}\right\}. \quad (19)$$

The currents flowing through the coils, which are the coefficients of vector $[I]$, can be obtained by (18) and are used to calculate the magnetic field. Additionally, the optimal value of the voltage source vector $[V_S]$ can also be derived to minimize the average magnetic field in a given region.

To calculate the magnetic field, the linearity assumption is adopted so that the principle of superposition holds and the number of field simulations is significantly reduced.

Let us indicate $\boldsymbol{b}_i^{(k)}$, the magnetic flux density in a generic k-th point, produced by a unit current $I_i = 1$ A through the i-th coil, with no currents in other coils (that is, $I_k = 0$, with $k \neq i$). This function can be expressed in Cartesian coordinates as

$$\boldsymbol{b}_i^{(k)} = \left(\boldsymbol{b}_i^{(k)} \cdot \hat{\mathbf{x}}\right)\hat{\mathbf{x}} + \left(\boldsymbol{b}_i^{(k)} \cdot \hat{\mathbf{y}}\right)\hat{\mathbf{y}} + \left(\boldsymbol{b}_i^{(k)} \cdot \hat{\mathbf{z}}\right)\hat{\mathbf{z}} = b_{i,x}^{(k)}\hat{\mathbf{x}} + b_{i,y}^{(k)}\hat{\mathbf{y}} + b_{i,z}^{(k)}\hat{\mathbf{z}} \tag{20}$$

where $\hat{\mathbf{x}}, \hat{\mathbf{y}}, \hat{\mathbf{z}}$ are the unit vectors along the coordinate axes.

When considering M points with $k = 1, 2, \ldots, M$, we can create 3 column vectors $[b_{i,x}]$, $[b_{i,y}]$, and $[b_{i,z}]$, one for each component, containing the Cartesian components of the field produced by the i-th current in the M selected points.

By applying superposition, the magnetic flux density produced by the coil current vector $[I]$ can be expressed as

$$\begin{bmatrix}[B_x]\\ [B_y]\\ [B_z]\end{bmatrix} = \begin{bmatrix}[b_{1x}] & \cdots & [b_{Nx}]\\ [b_{1y}] & \ddots & [b_{Ny}]\\ [b_{1z}] & \cdots & [b_{Nz}]\end{bmatrix}[I] \tag{21}$$

where $[B_x]$, $[B_y]$, and $[B_z]$ are the Cartesian components vectors of the total magnetic flux density in the M considered points.

The average value of the squared norm of the magnetic flux density in the considered region is given by [17,18]

$${B_{av}}^2 = \frac{1}{M}\sum_{k=1}^{M}\left\|\mathbf{B}^{(k)}\right\|^2 = \frac{1}{M}\begin{bmatrix}[B_x]^* & [B_y]^* & [B_z]^*\end{bmatrix}\begin{bmatrix}[B_x]\\ [B_y]\\ [B_z]\end{bmatrix} \tag{22}$$

where the star apex represents the conjugate.

Equation (20) can be used in an optimization algorithm to calculate the value of the voltage source vector $[V_S]$ that permits the minimization of the magnetic flux density in the considered region. We start by defining [23,24]

$$\begin{bmatrix}[g_1] & \cdots & [g_N]\end{bmatrix} = \begin{bmatrix}[b_{1x}] & \cdots & [b_{Nx}]\\ [b_{1y}] & \ddots & [b_{Ny}]\\ [b_{1z}] & \cdots & [b_{Nz}]\end{bmatrix}[Y_{eq}]. \tag{23}$$

The voltage source vector $[V_S]$ can be expressed as

$$[V_S] = \begin{bmatrix}1\\ 0\\ [\alpha_{SH}]\end{bmatrix}V_0 \tag{24}$$

where V_0 is the voltage source applied to the primary coil of the WPT system and $[\alpha_{SH}]$ is a $N-2$ column vector containing the gains of the controlled voltage sources applied to the $N-2$ shielding coils, which are assumed to depend on the primary voltage source, V_0 [19,20]. By adopting this notation, (22) can be rewritten as

$${B_{av}}^2 = \frac{1}{M}\left([g_1] + \begin{bmatrix}[g_3] & \cdots & [g_N]\end{bmatrix}[\alpha_{SH}]\right)^*\left([g_1] + \begin{bmatrix}[g_3] & \cdots & [g_N]\end{bmatrix}[\alpha_{SH}]\right)|V_0|^2. \tag{25}$$

For an optimization procedure, the objective function can be the minimization of B_{av}. This goal can be achieved by imposing [17,18]

$$[g_1] + \begin{bmatrix}[g_3] & \cdots & [g_N]\end{bmatrix}[\alpha_{SH}] = [0] \tag{26}$$

therefore, making sure that [19,20]

$$[\alpha_{SH}] = -\begin{bmatrix}[g_3] & \cdots & [g_N]\end{bmatrix}^{\dagger}[g_1] \tag{27}$$

where the operator † is the symbol of the pseudoinverse matrix, which is a generalization of the inverse matrix that provides a best-fit solution to linear equation systems.

Equation (25) provides the gains of the controlled voltage sources that need to be applied to the shielding coils in order to minimize the average magnetic field. Finally, the voltage source of the i-th active coil with $i = 3, 4, \ldots, N$ is given by

$$V_{SH,i} = \alpha_{SH,i} V_0. \tag{28}$$

In WPT systems, the power transfer efficiency η is traditionally calculated as the ratio of the real power at the output port, P_2, to the real power at the input port, P_1:

$$\eta = \frac{P_2}{P_1} \tag{29}$$

In the presence of active shielding coils, η is calculated as

$$\eta = \frac{P_1 - \sum_{i=1}^{N} P_{loss,i}}{P_1} \tag{30}$$

where $P_{loss,i}$ represents the power loss in the i-th coil [4].

The described procedure is highly effective for calculating the average magnetic induction value, B_{av}, in a region discretized into a grid of points. If the points are located on a surface, S, it becomes straightforward to compute the magnetic flux as $\boldsymbol{\phi} = B_{av}\, S$. Consequently, the induced electromotive force (*emf*) can be determined in a circuit whose path aligns with the contour of the surface, expressed as $emf = -j\boldsymbol{\omega\phi}$. This capability is crucial for evaluating induced effects on transmission lines and various types of circuits, facilitating the prediction of electromagnetic interference (EMI).

If the surface, S, is relatively small, for instance 100 cm^2, such as that of a magnetic field probe, this method can be employed to predict the maximum (*rms*) magnetic flux density at a specific point. This approach is recommended by SAE J2954 for evaluating compliance with the reference levels specified in ICNIRP 2010 [31] and ISO 14117 [32] for electromagnetic interference (EMI) limits in cardiac implantable electronic devices (CIEDs), which are set at 27 μT and 15 μT at 85 kHz, respectively.

3. Applications

3.1. WPT Systems

The performances and the magnetic field emission are calculated using a demonstrative WPT system. For this test, the worst operational condition is adopted. The maximum ground clearance level, Z3, allowed by the SAE J2954 standard is taken into account, with an air gap between the coils in the range 170–250 mm. A larger air gap is the condition in which the coupling factor is smaller and, therefore, the leakage flux is larger. The GA coil is supposed to be flush mounted in the ground ($z = 0$).

Figure 3 shows the configuration of the GA coil, which consists of a planar spiral coil made of two parallel copper litz wires, each with $N_1 = 8$ turns. The external dimensions of the coil are $w_1 = 500$ mm and $l_1 = 650$ mm. Two planar shields are placed under the coil. A ferrite shield, with the dimensions of $w_{1f} = 500$ mm and $l_{1f} = 650$ mm and a thickness of $t_k = 5$ mm, is used to enhance the magnetic coupling, while an aluminum shield, with

the dimensions of w_{1a} = 700 mm and l_{1a} = 900 mm and a thickness of t_k = 2 mm, is used to reduce the magnetic field.

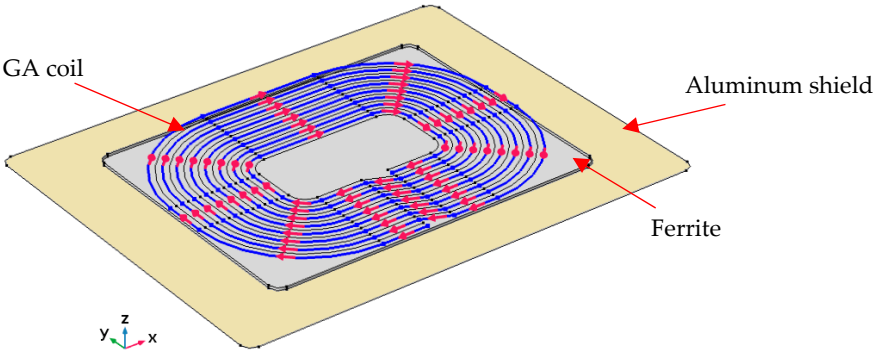

Figure 3. Electro-geometrical configuration of the GA coil.

The VA coil, shown in Figure 4, is mounted under a metal mimic pan that simulates the presence of the conductive bodyshell of the vehicle. The square coil, with sides of s = 380 mm, consists of a planar spiral coil made of a single copper litz wire with N_2 = 8 turns. A square ferrite shield, with sides of s_f = 380 mm and a thickness of t_k = 5 mm, is adopted to enhance magnetic coupling. Additionally, an aluminum shield, with the dimensions of w_{2a} = 700 mm and l_{2a} = 900 mm and a thickness of t_k = 2 mm, is used to reduce the magnetic flux leakage.

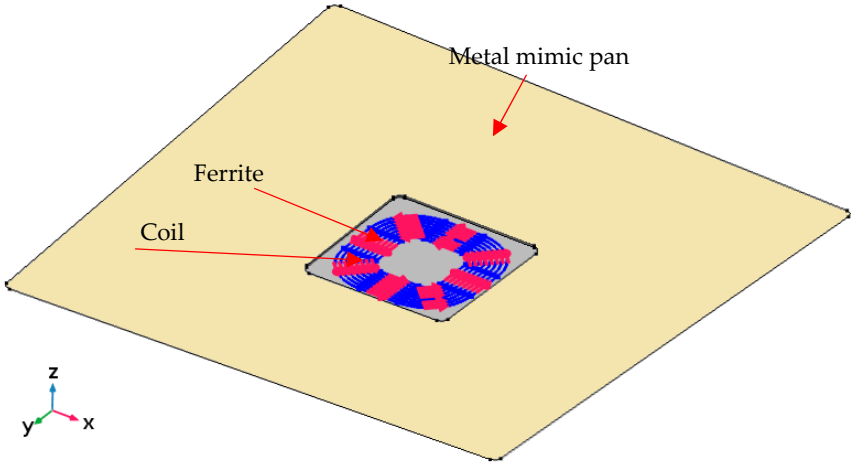

Figure 4. Electro-geometrical configuration of the VA coil.

The operational frequency is f = 85 kHz; the output power is fixed to P_2 = 7.7 kVA (SAE Power Class 2); and the output voltage is fixed to 400 V. The system is terminated on a load resistor, R_L = 10 Ω. For the sake of brevity, only the LCC compensation is considered as it is the most suitable for the coil configuration being considered [29].

The car body is simulated by a square metal mimic pan, with a side length of l_{mp} = 1.5 m. It is made of aluminum, with an electrical conductivity of σ = 37 MS/m and a thickness of t_k = 2 mm. The mimic pan is placed at a distance of d = 2 mm over the VA coil.

The maximum misalignment between the coils is used in this investigation: a front–back offset of Δx = 75 mm; a lateral offset of Δy = 100 mm; and a vertical separation between the GA and the VA coils of Δz = 250 mm. This coil configuration represents the worst-case scenario, according to the SAE standard for the power class considered.

The currents flowing in the GA and VA coils are regarded as being the sources of the magnetic field. Subsequently, three configurations of the active shielding coils are defined, featuring two, four, and six shielding coils positioned around the GA coil, as illustrated

in Figure 5. It is assumed that the shielding coils have, in all cases, only one turn. All the coils (WPT and shielding) are constructed from the same litz wire (AWG 38), composed of 1260 insulated strands [30].

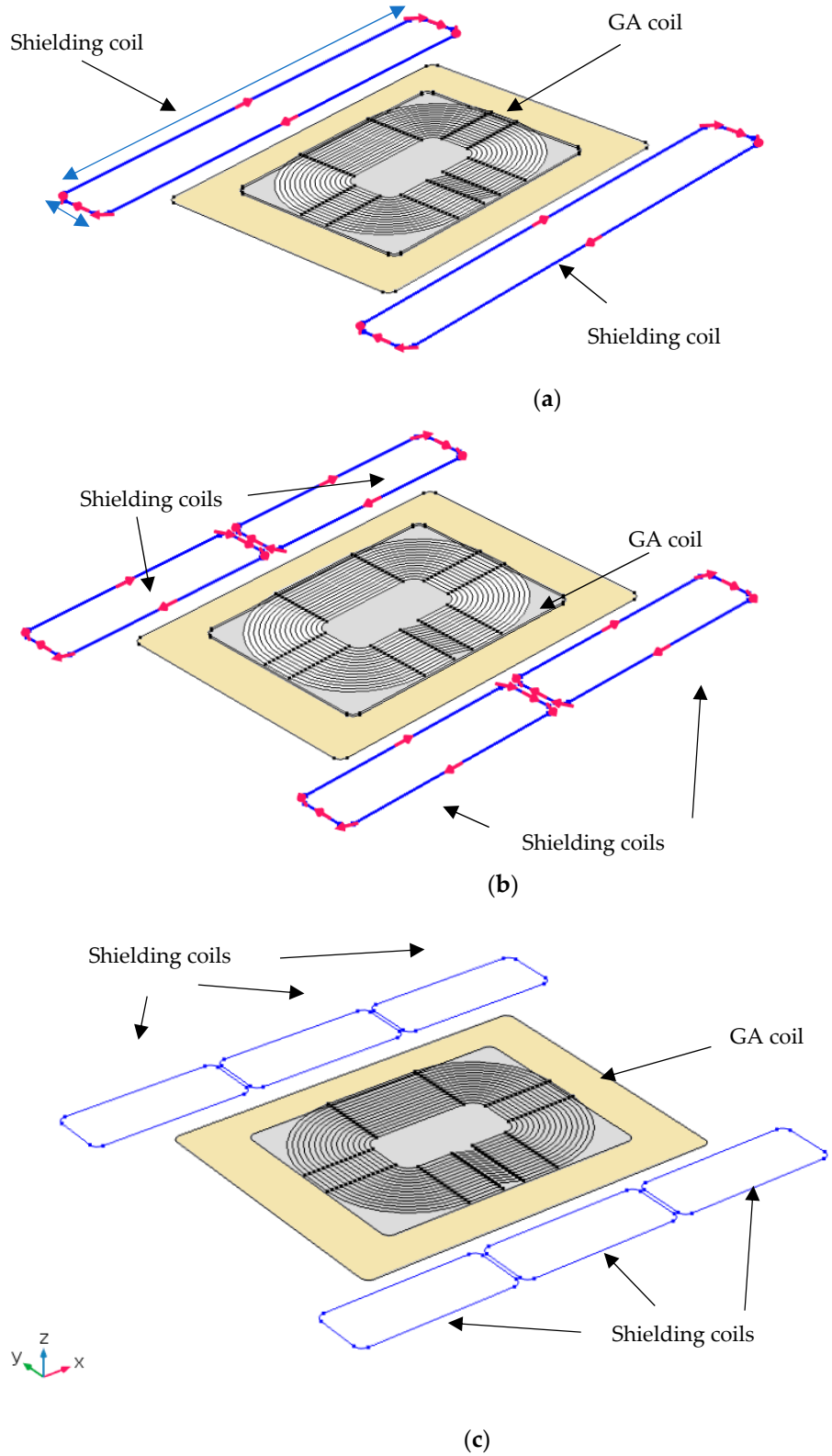

Figure 5. Proposed active shielding coil configuration: 2 coils (**a**), 4 coils (**b**), and 6 coils (**c**).

3.2. Electrical Performances

The self- and mutual inductances of the equivalent circuit are calculated by (1) and (2), respectively, using a 3D numerical simulation software for all configurations considered. The AC resistances of all the coils are taken from the litz wire datasheet at 85 kHz [30]. The obtained circuit parameters for the WPT coils are reported in Table 1.

Table 1. Equivalent circuit parameters without active shielding coils.

L_1 (μH)	L_2 (μH)	M_{12} (μH)	R_1 (mΩ)	R_2 (mΩ)
47.86	39.93	4.00	22.22	31.51

The procedure described in the previous section is then applied to all the shielding coil structures. The grid of points used as an input of the algorithm are taken on surfaces S_1 and S_2 placed on the exterior of the mimic pan, as shown in Figure 6. All the surfaces have a size of 1.5 m along x and 0.8 m along z and are placed at a distance of d_s = 0.8 m from the center of the mimic pan.

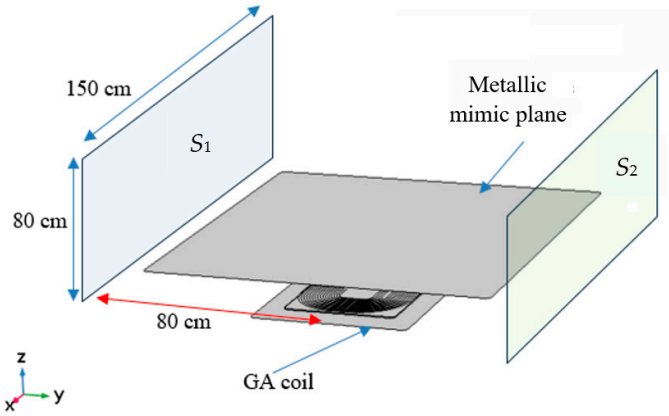

Figure 6. Surfaces S_1 and S_2 beside the WPT coil configuration where the average magnetic flux induction is calculated.

The result of the procedure is the assessment of the vector $[\alpha_{sh}]$ in (25). The obtained coefficients of $[\alpha_{sh}]$ for the three active shielding configurations considered are reported in Table 2. The WPT currents and efficiency obtained with active shielding coils are compared with those without them, and the results are reported in Table 3.

Table 2. Coefficients of $[\alpha_{SH}]$ for the three active shielding coil configurations with maximum misalignment.

	α_{SH}
2 active shielding coils	$-1.9091 \times 10^{-3} + j12.7359 \times 10^{-3}$ $-1.6459 \times 10^{-3} + j1.6536 \times 10^{-3}$
4 active shielding coils	$-1.0114 \times 10^{-3} + j3.0928 \times 10^{-3}$ $-8.0523 \times 10^{-6} + j705.1594 \times 10^{-6}$ $2.8947 \times 10^{-3} + j6.0339 \times 10^{-3}$ $1.7971 \times 10^{-3} + j16.3283 \times 10^{-3}$
6 active shielding coils	$1.2087 \times 10^{-3} + j1.2649 \times 10^{-3}$ $-1.8118 \times 10^{-3} + j5.1854 \times 10^{-3}$ $1.2390 \times 10^{-3} - j1.4751 \times 10^{-3}$ $5.7300 \times 10^{-3} - j4.8383 \times 10^{-3}$ $3.4344 \times 10^{-3} + j22.8283 \times 10^{-3}$ $8.4429 \times 10^{-3} + j7.4163 \times 10^{-3}$

Table 3. System performances with and without active shields.

	$\|I_1\|$ (A)	$\|I_2\|$ (A)	η (%)
Without active shielding	94.52	55.00	96.3
2 active shielding coils	94.22	55.00	96.1
4 active shielding coils	94.19	55.00	96.0
6 active shielding coils	94.23	55.00	95.8

3.3. Magnetic Field Mitigation

Finally, the obtained coil currents are used for calculating the magnetic field distribution. The field distribution is calculated in two parallelepiped volumes placed at the left and right of the mimic pan, at a distance of d_v = 50 mm from the mimic edge, as shown in Figure 7.

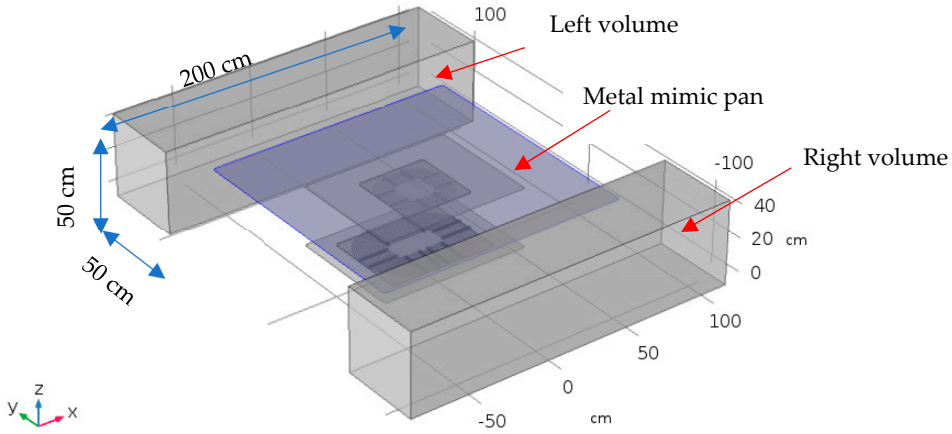

Figure 7. Volumes beside the WPT coil configuration where the magnetic flux induction is calculated.

The magnetic field distributions inside the volumes are depicted in Figure 8 for different active shielding coil configurations, and the maximum and average values of the magnetic flux density are reported in Table 4.

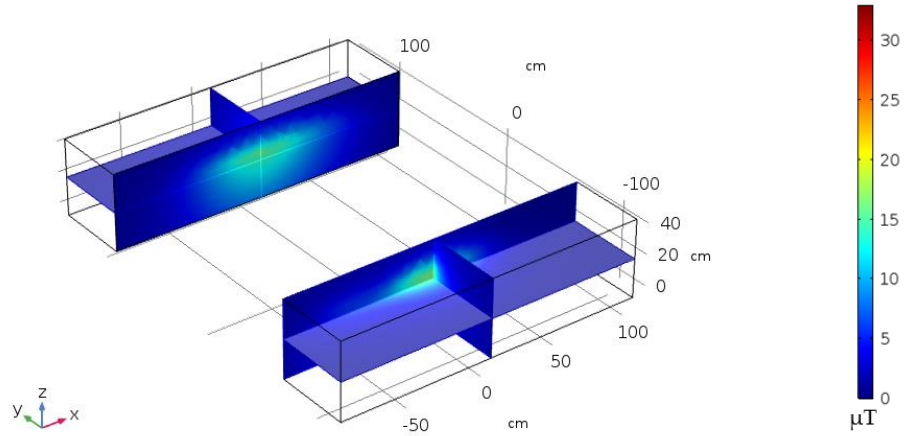

(**a**)

Figure 8. *Cont.*

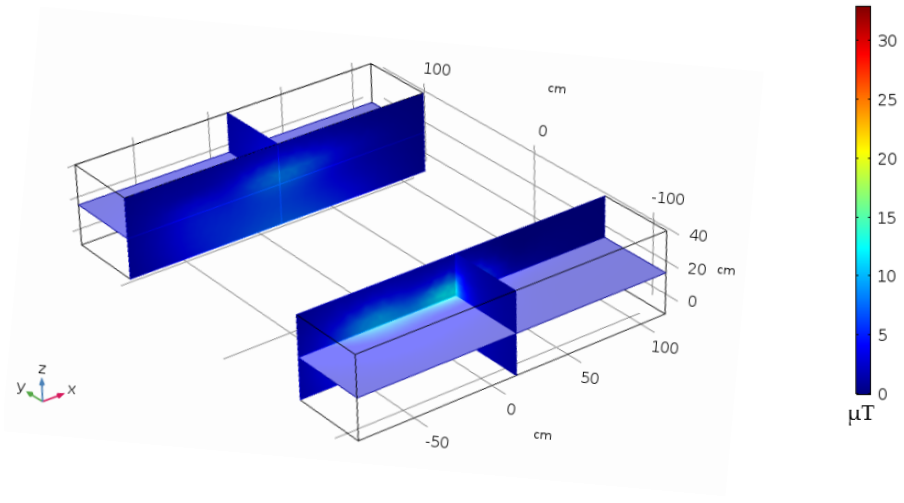

(**b**)

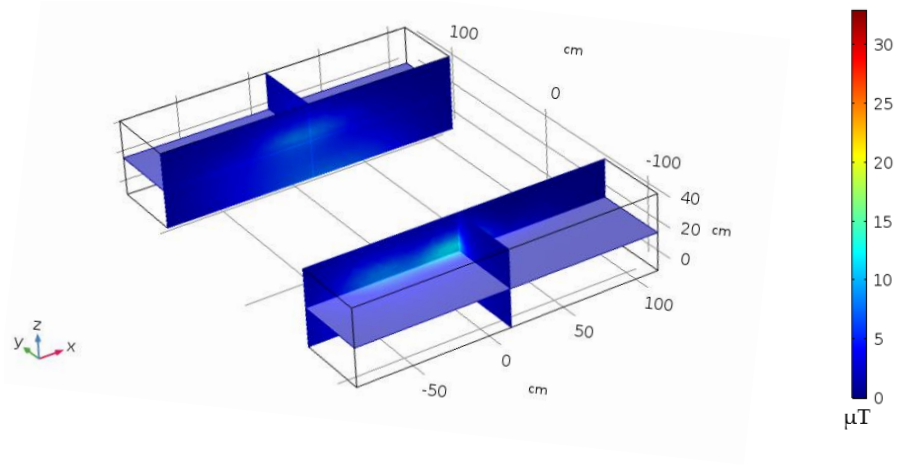

(**c**)

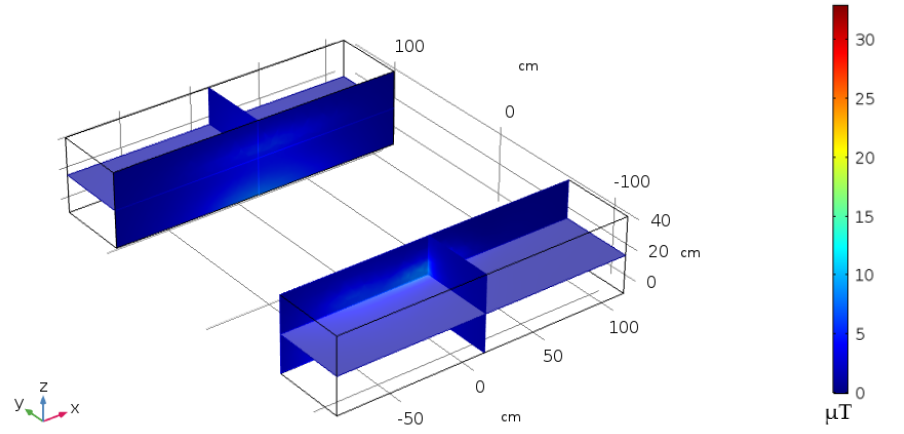

(**d**)

Figure 8. Distribution of the magnetic flux density *B* (rms) in the volumes without active shielding (**a**), with 2 active shielding coils (**b**), with 4 active shielding coils (**c**), and with 6 active shielding coils (**d**).

Table 4. Maximum and average magnetic flux density (*rms*) in the two volumes.

	Maximum B (μT)		Average B (μT)	
	Left Volume	**Right Volume**	**Left Volume**	**Right Volume**
No shielding coil	16.635	17.536	2.286	1.818
2 shielding coils	8.198	12.025	1.673	1.473
4 shielding coils	8.640	12.140	1.571	1.421
6 shielding coils	7.783	9.124	1.467	1.305

The obtained results highlight the significant reduction in the magnetic field achieved by adopting the proposed multicoil shielding configuration. The field in the considered area can be almost halved when six active shielding coils are used. Furthermore, using the six-coil configuration, it is possible to reduce the magnetic field where it is strongest, particularly in the central part of the reference volume (see Figure 8). In this set-up, the two central shielding coils offer superior shielding performance. In contrast, configurations with two or four shielding coils cannot target this specific goal as effectively.

Therefore, using two shielding coils is preferable for achieving a moderate reduction in the magnetic field, while the six-coil configuration allows for a more substantial reduction. In any case, the obtained values are well below the limits fixed by international regulations, such as the reference levels (RL) of the ICNIRP 2010 guidelines [31], and are also below the limit provided by SAE J2594 for people with cardiac implantable electronic devices (CIEDs) [32]. The RL, in terms of the magnetic flux induction at 85 kHz, is 27 μT, while the limit defined by ISO 14117 is set at 15 μT.

4. Conclusions

An innovative shielding solution based on an array of active coils for automotive wireless power systems has been presented. This approach effectively minimizes the magnetic field produced by a wireless charging system designed according to the SAE standard, while avoiding overall efficiency degradation, which is crucial for intentional magnetic field sources, such as WPT coils. The use of multiple shielding coils allows for precise field mitigation across the entire area around the system. The paper provides a detailed description of the theoretical and methodological aspects of an array of active shielding coils applied to a WPT system with double-sided LCC compensation, including the necessary equations, allowing the readers to easily apply the proposed method.

The effectiveness of the proposed procedure has been numerically tested considering the worst-case scenario for the wireless charging of EVs in terms of coil separation and misalignment. The results show that the magnetic field in the most critical areas beside the EV can be significantly reduced with a minimal drop in efficiency, even when accounting for the power needed by the shielding coils. The reduction in the power transfer efficiency was 0.3% when using two or four active coils and 0.5% when using six active coils. Meanwhile, the magnetic field was nearly halved in all tested configurations with the proposed arrays of active coils. Therefore, using four active coils represents the best compromise between maintaining efficiency and reducing the magnetic field. Future work will include the realization of a demonstrator to validate the system in a real scenario.

Finally, the proposed approach can be easily adapted for different configurations of WPT and shielding coils.

Author Contributions: S.C., T.C., F.M. and M.F. conceived and planned the simulations. S.C. and F.M. developed the algorithms. T.C. and M.F. realized the simulations set-up. All authors provided critical feedback, improved the final design, analyzed the data, and wrote the paper. All authors have read and agreed to the published version of the manuscript.

Funding: This research received no external funding.

Data Availability Statement: The original contributions presented in the study are included in the article, further inquiries can be directed to the corresponding author/s.

Conflicts of Interest: The authors declare no conflicts of interest.

References

1. Covic, G.A.; Boys, J.T. Inductive Power Transfer. *Proc. IEEE* **2013**, *101*, 1276–1289. [CrossRef]
2. Wang, C.-S.; Covic, G.A.; Stielau, O.H. Power Transfer Capability and Bifurcation Phenomena of Loosely Coupled Inductive Power Transfer Systems. *Trans. Ind. Electron.* **2004**, *51*, 148–157. [CrossRef]
3. Ahmad, A.; Alam, M.S.; Chabaan, R.A. Comprehensive Review of Wireless Charging Technologies for Electric Vehicles. *Trans. Transport. Electrific.* **2018**, *4*, 38–63. [CrossRef]
4. Feliziani, M.; Campi, T.; Cruciani, S.; Maradei, F. *Wireless Power Transfer for E-Mobility*, 1st ed.; Elsevier-Academic Press: Cambridge, MA, USA, 2023; ISBN 9780323995238.
5. Laporte, S.; Coquery, G.; Deniau, V.; De Bernardinis, A.; Hautière, N. Dynamic wireless power transfer charging infrastructure for future evs: From experimental track to real circulated roads demonstrations. *World Electr. Veh. J.* **2019**, *10*, 84. [CrossRef]
6. Buja, G.; Rim, C.T.; Mi, C.C. Dynamic Charging of Electric Vehicles by Wireless Power Transfer. *IEEE Trans. Ind. Electron.* **2016**, *63*, 6530–6532. [CrossRef]
7. Grazian, F.; Shi, W.; Soeiro, T.B.; Dong, J.; van Duijsen, P.; Bauer, P. Compensation Network for a 7.7 kW Wireless Charging System that Uses Standardized Coils. In Proceedings of the 2020 IEEE International Symposium on Circuits and Systems (ISCAS), Seville, Spain, 12–14 October 2020; pp. 1–5. [CrossRef]
8. Pahlavan, S.; Ashtiani, S.J. Rotation-Tolerant Wireless Power Transmission Scheme with Smart Positioning for Cognitive Research on Moving Animals. *IEEE Trans. Biomed. Circuits Syst.* **2024**, *18*, 123–130. [CrossRef] [PubMed]
9. De Santis, V.; Campi, T.; Cruciani, S.; Laakso, I.; Feliziani, M. Assessment of the Induced Electric Fields in a Carbon-Fiber Electrical Vehicle Equipped with a Wireless Power Transfer System. *Energies* **2018**, *11*, 684. [CrossRef]
10. Ding, P.; Bernard, L.; Pichon, L. Evaluation of Electromagnetic Field in Human Body Exposed to Wireless Inductive Charging System. *IEEE Trans. Magn.* **2014**, *50*, 1037–1040. [CrossRef]
11. Laakso, I.; Hirata, A. Evaluation of the induced electric field and compliance procedure for a wireless power transfer system in an electrical vehicle. *Phys. Med. Biol.* **2013**, *58*, 7583. [CrossRef]
12. Kim, J.; Kong, S.; Kim, H.; Suh, I.-S.; Suh, N.P.; Cho, D.-H.; Kim, J.; Ahn, S. Coil Design and Shielding Methods for a Magnetic Resonant Wireless Power Transfer System. *Proc. IEEE* **2013**, *101*, 1332–1342. [CrossRef]
13. Campi, T.; Cruciani, S.; Feliziani, M. Magnetic Shielding of Wireless Power Transfer Systems. In Proceedings of the 2014 International Symposium on Electromagnetic Compatibility (EMC'14), Tokyo, Japan, 12–16 May 2014; pp. 422–425.
14. Kim, S.; Park, H.-H.; Kim, J.; Kim, J.; Ahn, S. Design and Analysis of a Resonant Reactive Shield for a Wireless Power Electric Vehicle. *IEEE Trans. Microw. Theory Techn.* **2014**, *62*, 1057–1066. [CrossRef]
15. Ishida, M.; Watanabe, T. Magnetic Field Canceling Coil for Wireless Power Transfer System. In Proceedings of the 2015 IEEE Wireless Power Transfer Conference (WPTC), Boulder, CO, USA, 13–15 May 2015; pp. 1–4.
16. Park, J.; Kim, D.; Hwang, K.; Park, H.H.; Kwak, S.I.; Kwon, J.H.; Ahn, S. A Resonant Reactive Shielding for Planar Wireless Power Transfer System in Smartphone Application. *IEEE Trans. Electromagn. Compat.* **2017**, *59*, 695–703. [CrossRef]
17. Zhu, Q.; Zhang, Y.; Guo, Y.; Liao, C.; Wang, L.; Wang, L. Null-Coupled Electromagnetic Field Canceling Coil for Wireless Power Transfer System. *IEEE Trans. Transp. Electrific.* **2017**, *3*, 464–473. [CrossRef]
18. Mohammad, M.; Wodajo, E.T.; Choi, S.; Elbuluk, M.E. Modeling and Design of Passive Shield to Limit EMF Emission and to Minimize Shield Loss in Unipolar Wireless Charging System for EV. *IEEE Trans. Power Electron.* **2019**, *34*, 12235–12245. [CrossRef]
19. Cruciani, S.; Campi, T.; Maradei, F.; Feliziani, M. Active Shielding Design for Wireless Power Transfer Systems. *IEEE Trans. Electromagn. Compat.* **2019**, *61*, 1953–1960. [CrossRef]
20. Campi, T.; Cruciani, S.; Maradei, F.; Feliziani, M. Magnetic Field Mitigation by Multicoil Active Shielding in Electric Vehicles Equipped with Wireless Power Charging System. *IEEE Trans. Electromagn. Compat.* **2020**, *62*, 1398–1405. [CrossRef]
21. Scher, A.D.; Mohammad, M.; Ozpineci, B.; Onar, O. Design and Optimization of Cancellation Coil Topologies for a Ferrite-Less Wireless EV Charging Pad. In Proceedings of the 2021 IEEE Transportation Electrification Conference & Expo (ITEC), Chicago, IL, USA, 21–25 June 2021; pp. 1–7.
22. Qin, R.; Li, J.; Sun, J.; Costinett, D. Shielding Design for High-Frequency Wireless Power Transfer System for EV Charging with Self-Resonant Coils. *IEEE Trans. Power Electron.* **2023**, *38*, 7900–7912. [CrossRef]
23. Cruciani, S.; Campi, T.; Maradei, F.; Feliziani, M. Active Shielding Applied to an Electrified Road in a Dynamic Wireless Power Transfer (WPT) System. *Energies* **2020**, *13*, 2522. [CrossRef]
24. Cruciani, S.; Campi, T.; Maradei, F.; Feliziani, M. Active Shielding Design and Optimization of a Wireless Power Transfer (WPT) System for Automotive. *Energies* **2020**, *13*, 5575. [CrossRef]
25. Kim, H.; Song, C.; Kim, D.H.; Jung, D.H.; Kim, I.M.; Kim, Y.I.; Kim, J.; Ahn, S.; Kim, J. Coil design and measurements of automotive magnetic resonant wireless charging system for high-efficiency and low magnetic field leakage. *IEEE Trans. Microw. Theory Tech.* **2016**, *64*, 383–400. [CrossRef]

26. Li, Y.; Zhang, S.; Cheng, Z. Double-Coil Dynamic Shielding Technology for Wireless Power Transmission in Electric Vehicles. *Energies* **2021**, *14*, 5271. [CrossRef]
27. Tan, L.; Elnail, K.E.I.; Ju, M.; Huang, X. Comparative Analysis and Design of the Shielding Techniques in WPT Systems for Charging EVs. *Energies* **2019**, *12*, 2115. [CrossRef]
28. Choi, S.Y.; Gu, B.W.; Lee, S.W.; Lee, W.Y.; Huh, J.; Rim, C.T. Generalized Active EMF Cancel Methods for Wireless Electric Vehicles. *IEEE Trans. Power Electron.* **2013**, *29*, 5770–5783. [CrossRef]
29. *SAE J2954*; Wireless Power Transfer for Light-Duty Plug-in/Electric Vehicles and Alignment Methodology. Society of Automotive Engineers (SAE): Warrendale, PA, USA, 2022.
30. Available online: https://www.packlitzwire.com/products/litz-wires/rupalit-classic/ (accessed on 4 January 2024).
31. International Commission on Non-Ionizing Radiation Protection. Guidelines for limiting exposure to time-varying electric and magnetic fields for low frequencies (1 Hz–100 kHz). *Health Phys.* **2010**, *99*, 818–836. [CrossRef]
32. *ISO 14117:2019*; Active Implantable Medical Devices—Electromagnetic Compatibility—EMC Test Protocols for Implantable Cardiac Pacemakers, Implantable Cardioverter Defibrillators and Cardiac Resynchronization Devices. ISO: Geneva, Switzerland, 2019.